

# TreeQ: Pushing the Quantization Boundary of Diffusion Transformer via Tree-Structured Mixed-Precision Search

Kaicheng Yang<sup>1</sup>, Kaisen Yang<sup>2</sup>, Baiting Wu<sup>2</sup>,

Xun Zhang<sup>1</sup>, Qianrui Yang<sup>2</sup>, Haotong Qin<sup>3</sup>, He Zhang<sup>4</sup>, Yulun Zhang<sup>1\*</sup>

<sup>1</sup>Shanghai Jiao Tong University, <sup>2</sup>Tsinghua University, <sup>3</sup>ETH Zürich, <sup>4</sup>Adobe Research

## Abstract

*Diffusion Transformers (DiTs) have emerged as a highly scalable and effective backbone for image generation, outperforming U-Net architectures in both scalability and performance. However, their real-world deployment remains challenging due to high computational and memory demands. Mixed-Precision Quantization (MPQ), designed to push the limits of quantization, has demonstrated remarkable success in advancing U-Net quantization to sub-4-bit settings while significantly reducing computational and memory overhead. Nevertheless, its application to DiT architectures remains limited and underexplored. In this work, we propose **TreeQ**, a unified framework addressing key challenges in DiT quantization. First, to tackle inefficient search and proxy misalignment, we introduce **Tree-Structured Search (TSS)**. This DiT-specific approach leverages the architecture’s linear properties to traverse the solution space in  $\mathcal{O}(n)$  time while improving objective accuracy through comparison-based pruning. Second, to unify optimization objectives, we propose **Environmental Noise Guidance (ENG)**, which aligns Post-Training Quantization (PTQ) and Quantization-Aware Training (QAT) configurations using a single hyperparameter. Third, to mitigate information bottlenecks in ultra-low-bit regimes, we design the **General Monarch Branch (GMB)**. This structured sparse branch prevents irreversible information loss, enabling finer detail generation. Through extensive experiments, our **TreeQ** framework demonstrates state-of-the-art performance on DiT-XL/2 under W3A3 and W4A4 PTQ/PEFT settings. Notably, our work is the first to achieve near-lossless 4-bit PTQ performance on DiT models. The code and models will be available at <https://github.com/racoonykc/TreeQ>.*

## 1. Introduction

Model quantization has emerged as a key approach to mitigating the computational bottlenecks of diffusion models. Within existing quantization paradigms, particularly Post-Training Quantization (PTQ) [24, 28, 34, 51, 53, 54, 57]

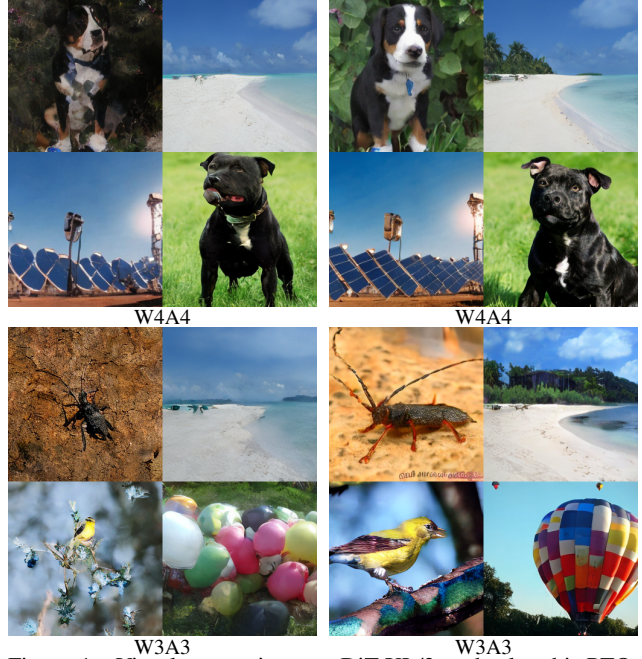


Figure 1. Visual comparison on DiT-XL/2 under low-bit PTQ. TreeQ achieves better generation compared to baseline [61].

and Quantization-Aware Training (QAT) [17, 18, 23, 33, 38, 56, 69, 70], allocating appropriate precision is critical. Uniform precision quantization often fails to accommodate the diverse activation distributions in diffusion models, which vary significantly across layers. This heterogeneity introduces redundancy: excessive precision for insensitive components wastes resources, while insufficient precision for sensitive components degrades performance.

Mixed-precision quantization (MPQ) addresses these issues by allocating different bit-widths to different model components, enabling flexible target average bit-widths and improved performance. However, existing MPQ approaches face major challenges: (i) proxy objectives often misalign with true performance metrics, leading to suboptimal assignments [17, 18, 52, 67], (ii) search procedures are computationally expensive [20, 32], and (iii) in extreme low activation bit regimes (e.g., 3-bit), MPQ suffers from propagation bottlenecks that cannot be recovered by simple low-rank auxiliary branches.

To overcome these challenges, we propose TreeQ, a uni-

\*Corresponding author: Yulun Zhang, yulun100@gmail.com

fied framework addressing each of these issues. First, to tackle inefficient search (ii) and proxy misalignment (i), we propose Tree-Structured Search (TSS), a search framework designed for DiT architectures. It leverages the linear properties of the DiT structure to efficiently traverse the mixed-precision solution space with  $\mathcal{O}(n)$  time complexity and improves search objective accuracy through a comparison-based pruning method. Second, to further address the objective misalignment (i) between different quantization schemes, we introduce Environmental Noise Guidance (ENG). This method guides the optimization objective within the TSS framework to favor either PTQ or QAT via a simple hyperparameter. Third, to break the propagation bottlenecks (iii) in low-bit regimes, we introduce the General Monarch Branch (GMB). This structured sparse matrix branch overcomes irreversible information loss caused by low-bit quantization and low-rank branches, enabling finer detail generation. Extensive experiments and ablation studies demonstrate the effectiveness of each component, which collectively advance the state-of-the-art towards lower-bit and more practical DiT models.

Our main contributions are:

- We introduce **TSS**, a search framework designed for DiT architectures that efficiently explores the mixed-precision solution space with  $\mathcal{O}(n)$  time complexity for  $n$ -layer models. It enhances search objective accuracy through comparison-based bottom-up merging and pruning.
- We introduce **ENG**, which guides the optimization objective within the TSS framework to favor either PTQ or QAT via a simple hyperparameter.
- We introduce **GMB**, a structured sparse matrix branch that overcomes irreversible information loss caused by low-bit quantization and standard low-rank branches, enabling finer detail generation in quantized models.
- Our proposed framework, **TreeQ**, achieves state-of-the-art performance on DiT-XL/2 under W3A3 and W4A4 PTQ/PEFT settings, and is the first to achieve near-lossless 4-bit PTQ performance on DiT-XL/2.

## 2. Related Work

**Quantization of Diffusion Models.** Diffusion Models (DMs) have demonstrated strong generative capabilities across vision and multimodal tasks [5, 6, 21, 22, 26, 27, 36, 37, 39, 40, 46, 47, 68]. To improve scalability and generality, recent works replace the traditional U-Net [48] with Transformer architectures [55] [7, 47, 62]. Diffusion Transformers (DiTs) [46] achieve strong performance; however, their inference remains expensive in both memory and computation, limiting practical deployment. To reduce inference cost, post-training quantization (PTQ) methods [34, 51] reconstruct activations using calibration, while subsequent work improves temporal robustness and efficiency [24, 53, 54]. Transformer-based DMs further adopt

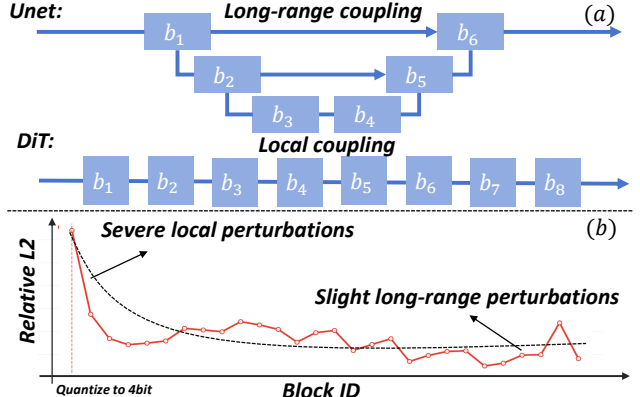


Figure 2. Analysis of DiT’s local coupling properties. (a) U-Net’s skip connections create long-range dependencies, whereas DiT exhibits a simple linear structure of block connections. (b) Relative L2 loss versus distance when quantizing the first block’s attn.qkv layer to 4-bit. This inspires our tree-structured merging algorithm, which progressively aggregates local segments into global configurations while ensuring evaluation of each adjacency relationship.

salience-guided calibration [28, 57]. A core challenge remains handling outliers: methods such as SVDQuant [33] and EfficientDM [23] mitigate them using LoRA, whereas TRDQ [52], RobuQ [61], and HadaNorm [15] leverage orthogonal transforms. On the quantization-aware training (QAT) side, Q-dm [38], BinaryDM [70], and BiDM [69] achieve ultra-low bit regimes, while QuEST [56] and EfficientDM [23] reduce fine-tuning costs.

**Mixed-Precision Quantization.** Mixed-precision quantization (MPQ) assigns heterogeneous bit-widths to model components to reflect non-uniform sensitivity under resource constraints. In large language models (LLMs), AMQ [32] uses AutoML for layer-wise bit selection, while LLM-MQ adopts gradient-based sensitivity with constrained optimization. For Vision Transformers, FIMA-Q [58] and APHQ-ViT [59] employ Fisher-based or Hessian-based sensitivity metrics to guide low-bit reconstruction. For diffusion models, methods such as Mix-DQ [67], MPQ-DM [17], MPQ-DMv2 [18], Mix-DiT [30] and Qua2SeDiMo [20] investigate mixed-precision planners based on integer programming and GNN-based search. These studies suggest that adaptive bit-width assignment is effective for maintaining performance at low bit setting.

**Structured Sparse Matrices.** Structured sparse matrices aim to achieve both hardware efficiency and parameter reduction on modern accelerators [8, 16, 64, 71, 72]. Early work in this direction includes Butterfly matrices [35], which are highly expressive but can be hardware-inefficient in practice. To address this limitation, hardware-aware variants such as Pixelated Butterfly [9] were subsequently developed. A prominent example in this line of work is the Monarch matrix [10], parameterized as a product of two block-diagonal matrices. This structure maps efficiently

to hardware-native BMM routines [14, 19, 42] and, importantly, enables optimal initialization from pre-trained dense weights via an analytical projection.

### 3. Methodology

#### 3.1. Preliminary

In this section, we first describe the baseline quantization procedure [61] used in our framework, which has demonstrated state-of-the-art (SOTA) performance.

**Activation Quantization.** Let  $\mathbf{X} \in \mathbb{R}^{T \times C}$  be token activations. Applying  $\mathbf{H}_C$  yields  $Y_{t,c} = \sum_j (\mathbf{H}_C)_{j,c} X_{t,j}$ . By generalized CLT,  $Y_{t,.}$  approaches  $\mathcal{N}(0, \sigma_t^2)$ , where  $\sigma_t^2 = \frac{1}{C} \sum_j \text{Var}(X_{t,j})$ . The transformed activations are then quantized in the Gaussian domain using a high-bit **symmetric** uniform quantizer  $Q_{\text{uni}}(\cdot)$ . This quantizer utilizes a pre-computed optimal  $\delta$ , determined for the standard normal distribution  $\mathcal{N}(0, 1)$ , and is designed for efficient deployment on INT operators:

$$Q_G(\mathbf{x}) = \sigma_t \cdot Q_{\text{uni}}\left(\frac{\mathbf{H}_n^\top \mathbf{x}}{\sigma_t}\right). \quad (1)$$

**Weight Quantization.** Given a weight matrix  $\mathbf{W} \in \mathbb{R}^{m \times n}$ , we first apply a normalized Hadamard transform  $\mathbf{H}_n$  to obtain the transformed weight  $\mathbf{W}_H = \mathbf{W}\mathbf{H}_n$ , and perform SVD on it while explicitly retaining a rank- $r$  ( $r=16$ ) full-precision component:

$$\mathbf{W}_H \approx \mathbf{A}\mathbf{B} = \mathbf{U}_r \mathbf{\Sigma}_r \mathbf{V}_r^\top. \quad (2)$$

The residual  $\mathbf{W}_{\text{res}} = \mathbf{W}_H - \mathbf{A}\mathbf{B}$  is then quantized channel-wise, leveraging the same symmetric uniform quantizer  $Q_{\text{uni}}(\cdot)$  from activation quantization:

$$Q_w(\mathbf{W}_{\text{res}}) = \sigma_c \cdot Q_{\text{uni}}\left(\frac{\mathbf{W}_{\text{res}}}{\sigma_c}\right). \quad (3)$$

where  $\sigma_c$  is the channel-wise standard deviation of the residual  $\mathbf{W}_{\text{res}}$ . The final reconstructed weight is:

$$\hat{\mathbf{W}} = \underbrace{(\mathbf{A}\mathbf{B} + Q_w(\mathbf{W}_{\text{res}}))}_{\text{LRB}} \mathbf{H}_n^\top. \quad (4)$$

where  $\mathbf{Q}_w$  is the quantized residual.

#### 3.2. Tree-Structured Search (TSS)

##### 3.2.1. Main Issues in Current Methods

We found that there are several remaining unsolved issues in current mixed-precision quantization for DiTs:

- **Under-utilization of DiT Topology.** Unlike U-Nets that contain global shortcut structures, DiTs are strictly linear. As shown in Fig. 2, neighboring blocks in DiT exhibit much stronger mutual dependencies. Current methods fail to leverage this structural prior.
- **Objective Misalignment.** Most existing layer-wise heuristic methods define sensitivity at the layer level, and then search configurations by minimizing a heuristic objective under a target bit budget. However, such heuristics

ignore inter-layer interactions, resulting in objective misalignment and severe suboptimality in PTQ.

- **Excessive Complexity.** ML-based configuration search requires auxiliary models and curated training data, thus complex, difficult to implement, and non-generalizable; enumeration or evolutionary approaches depend on high-quality metrics and are computationally prohibitive.

Motivated by these limitations, we aim to develop an algorithm that (i) fully exploits the locality induced by DiT’s linear topology (ii) operates via comparisons to eliminate reliance on expensive metrics and avoid objective misalignment (iii) achieves controllable time complexity that scales gracefully with model depth.

##### 3.2.2. Formal Description for TSS

**Definitions.** The DiT backbone is an ordered sequence of weights  $\{w_i\}_{i=1}^N$ . Any consecutive subsequence  $m = \{w_i\}_{i=p}^q$  is a *module*.

A *configuration*  $c_I$  for module  $m$  with index set  $I$  specifies the quantization bitwidth for each weight in the module, denoted as  $c_I = \{b_i\}_{i \in I}$  where  $b_i$  is the bitwidth assigned to weight  $w_i$ . The *mean bitwidth*  $\bar{c}(c_I)$  is defined as the FLOPs-weighted average across all weights in the module.

An *environment*  $e$  specifies default bitwidths for layers outside  $m$ . Given a configuration  $c_m$  under environment  $e$ ,  $p_e(c_m)$  denotes a real-valued *performance indicator*.

For a candidate set  $S_m = \{c_j\}_{j=1}^K$  on module  $m$ , the *Pareto queue*  $P_{(p,e)}(S_m)$  consists of non-dominated configurations with respect to  $(p, \bar{c})$ :

$$\begin{aligned} c \in P_{(p,e)}(S_m) &\iff \neg \exists c' \in S_m \\ \text{s.t. } [p_e(c') \leq p_e(c)] \wedge [\bar{c}' \leq \bar{c}]. \end{aligned} \quad (5)$$

where at least one of the inequalities is strict.

If two queues correspond to disjoint modules  $m_1, m_2$ , their *Cartesian* is defined as

$$\begin{aligned} P_{(p,e)}(S_{m_1}) \otimes P_{(p,e)}(S_{m_2}) &:= \\ P_{(p,e)}(\{c_i \cup c_j \mid c_i \in S_{m_1}, c_j \in S_{m_2}\}). \end{aligned} \quad (6)$$

Notably, this procedure relies only on relative comparisons of local structures, requiring the performance indicator to preserve the local ordering of configurations. This allows the use of inexpensive calibration MSE.

**TSS procedure.** Figure 3 illustrates the hierarchical pipeline. We first treat each layer as a node and enumerate all admissible bitwidths to form its local Pareto queue. Following DiT’s linear topology, we iteratively merge *adjacent* nodes: for each neighboring pair, we take the Cartesian of their Pareto queues. As shown in Fig. 3, the Cartesian product remains extremely sparse:

$$|P_{(p_1,e)}(S_{m_1}) \otimes P_{(p_2,e)}(S_{m_2})| \ll |S_{m_1}| \cdot |S_{m_2}|, \quad (7)$$

ensuring that queue sizes remain small during bottom-up merging. If a merged queue exceeds the maximum size  $k$ , we retain only the top  $k$  candidates whose mean bitwidths are closest to the target. This process continues until

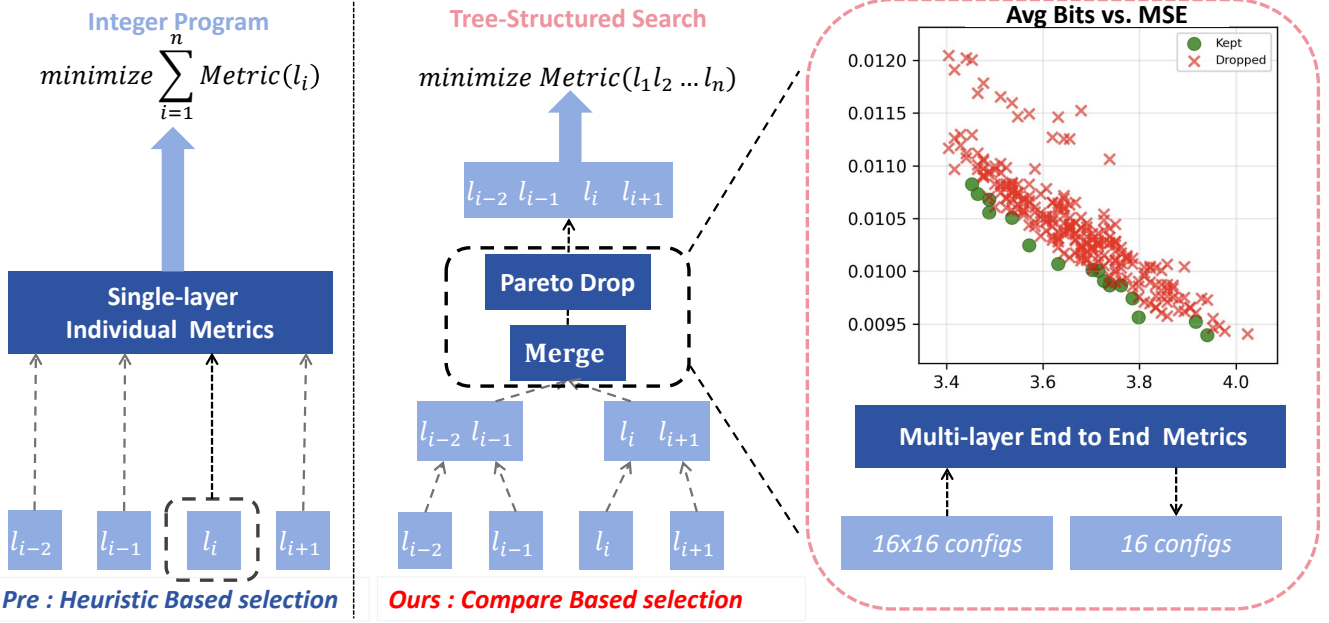


Figure 3. Visualization comparison between TSS and traditional methods Integer Programming. **(left)** Integer programming methods typically define a layer-wise heuristic function and set the optimization goal as minimizing the sum of these functions. This implies a necessary linearity between the heuristic and final performance, leading to an optimization objective error. **(right)** TSS leverages DiT's local coupling, merging the search strategy from local to global. This naturally considers the interactions between multiple layers and allocates more resources to strongly coupled adjacent layers. By adopting a comparison-based Pareto queue pruning strategy, the chosen objective function (e.g., MSE) only needs to be strongly order-preserving with the final performance, correcting the optimization objective.

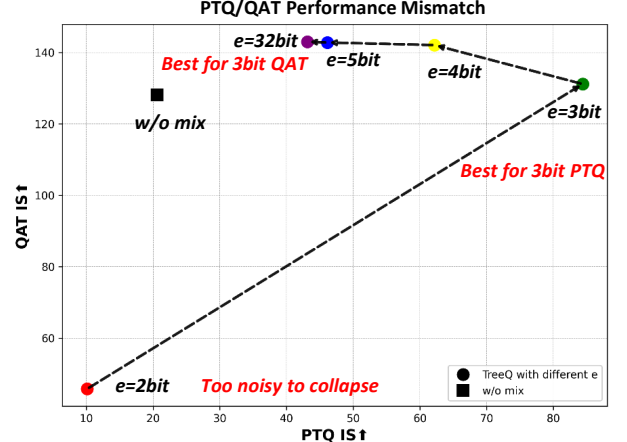
a single root queue remains, representing globally non-dominated candidates. The final configuration is chosen as the one whose mean bitwidth  $\bar{c}$  is closest to the target  $c_{\text{target}}$ .

In Supplementary Material, we show that if a single indicator evaluation costs  $\alpha$ , the Pareto queue size is  $k$ , and the model has  $n$  layers, then TSS runs in  $\mathcal{O}(\alpha k^2 n)$ , achieving controllable linear scaling with model depth. Notably, exactly  $n - 1$  merging steps occur, corresponding precisely to the  $n - 1$  local connections in the original DiT, naturally accounting for its strong local dependencies.

### 3.2.3. Environment Noise Guidance

**PTQ vs. QAT objectives.** PTQ and QAT have distinct objectives. For PTQ, the model cannot fine-tune away errors, so each layer must accommodate the macroscopic noise introduced by others. Traditional integer programming (IP) methods, however, often evaluate layers in a noise-free environment. While this isolates layer sensitivity, it ignores the inter-layer error propagation that causes catastrophic failure in PTQ. This noise-free evaluation is actually more suitable for QAT, where gradient-based fine-tuning aligns the quantized layers back toward full precision.

**Unifying Objectives via Environment Noise Guidance.** To unify these objectives, we introduce **Environment Noise Guidance (ENG)** within the TSS framework. ENG uses a simple hyperparameter  $e$  to simulate the target context. As shown in Fig. 4, this parameter is highly sensitive. For PTQ, we inject realistic noise by setting  $e$  to the target bit-width,



forcing the search to find a robust strategy. For QAT, we minimize noise ( $e=32\text{bit}$ ) to find strategies best suited for fine-tuning. This flexibility in adapting to distinct quantization objectives (PTQ and QAT) via a single parameter,  $e$ , underscores the versatility design of the TSS framework.

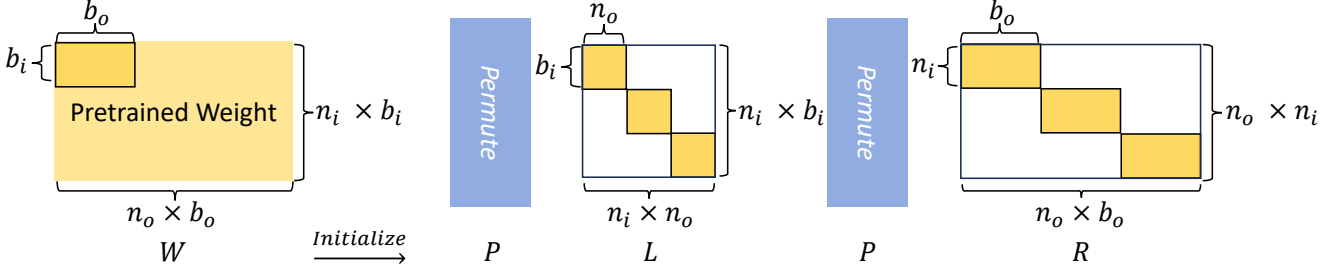


Figure 5. Visualization of GMB. GMB can initialize a structured sparse matrix with arbitrary sparsity from a pre-trained weight of any shape. The block-diagonal form of the sub-matrices facilitates efficient parallel processing on modern GPUs.

### 3.3. General Monarch Branch

#### 3.3.1. Issue of Local High-Frequency Information

In many low-bit quantized diffusion models, we observe a consistent phenomenon: global metrics such as FID [25] often remain reasonable, while spatial FID (sFID) [44], which evaluates local structure fidelity, deteriorates significantly. This discrepancy becomes more pronounced in ultra-low-bit quantization (e.g., 2-bit or 3-bit), indicating that while global, low-frequency information is largely preserved, fine-grained high-frequency details are substantially degraded. Such local information loss can adversely impact visual fidelity, especially for structured features critical for downstream perception. A straightforward remedy is to increase the rank of low-rank branches. However, this approach is counterproductive for quantization: since parameter count grows linearly with rank, higher rank requires substantially much more parameters, directly opposing the goal of model compression. Alternatively, one may introduce sparse high-rank skip connections, but existing variants are typically *unstructured* (e.g., top- $k$  element selection) [41] and misaligned with hardware-native block BMM kernels.

#### 3.3.2. General Monarch Matrices

This motivates another direction: introducing a parallel *structured sparse high-rank branch*, which is (i) **high-rank** enough to inject the missing local residuals, and (ii) **block-structured** to inherit the same kernel efficiency as standard block BMM. We take inspiration from Monarch matrices [10], and generalize the original *square-only* design to a block-partitioned form applicable to arbitrary weight shapes, yielding the **General Monarch Branch (GMB)**.

#### 3.3.3. General Monarch Decomposition

Let  $A \in \mathbb{R}^{N_o \times N_i}$  be a weight matrix. We first partition the input and output dimensions into blocks:

$$N_i = n_i \cdot b_i, \quad N_o = n_o \cdot b_o, \quad (8)$$

defining  $n_o \times n_i$  sub-matrices

$$M_{jk} \in \mathbb{R}^{b_o \times b_i}, \quad j = 1, \dots, n_o, \quad k = 1, \dots, n_i. \quad (9)$$

The full matrix can be reconstructed exactly as

$$A = \text{concat}_{j,k} M_{jk}, \quad (10)$$

where  $\text{concat}_{j,k}$  denotes concatenation along rows and columns.

Each block  $M_{jk}$  is then approximated by a rank-1 decomposition

$$M_{jk} \approx u_{jk} v_{jk}^\top, \quad u_{jk} \in \mathbb{R}^{b_o}, \quad v_{jk} \in \mathbb{R}^{b_i}. \quad (11)$$

Aggregating all rank-1 factors constructs the core Monarch tensors by grouping the components dimension-wise:

$$L'[j, k, :] = u_{jk} \in \mathbb{R}^{b_o}, \quad R'[j, k, :] = v_{jk} \in \mathbb{R}^{b_i}, \quad (12)$$

for  $j = 1, \dots, n_o$  and  $k = 1, \dots, n_i$ . Using the Monarch permutation matrix  $P$  [10], we transform this representation into a more efficient and compact factored form:

$$\hat{M} = PLPR, \quad (13)$$

where the factor matrices  $L \in \mathbb{R}^{n_o b_o \times n_i n_o}$  and  $R \in \mathbb{R}^{n_i n_o \times n_i b_i}$  are obtained by reshaping and permuting  $L'$  and  $R'$  to expose their block-diagonal structure, as illustrated in Fig. 5, which provides a clear visualization.

To match the parameter budget of a low-rank branch  $AB$  with rank  $r$ , the parameter counts must satisfy:

$$n_i n_o (b_i + b_o) = r(n_o b_o + n_i b_i). \quad (14)$$

A simple and valid solution to this constraint is to set  $n_i = n_o = r$ . Consequently, in our experiments, we enforce this configuration where both the row and column partition counts are set to  $r$  to achieve effective sparsity control while maintaining computational tractability.

#### 3.3.4. Quantization with GMB

Let  $\mathbf{W}_H = \mathbf{W}\mathbf{H}_n$  denote the Hadamard-transformed weight matrix. In the transformed domain,  $\mathbf{W}_H$  is decomposed into LRB, GMB and quantized residual:

$$\mathbf{W}_{\text{res}} = \mathbf{W}_H - AB - PLPR, \quad (15)$$

$$\hat{\mathbf{W}}_H = \underbrace{AB}_{\text{LRB}} + \underbrace{PLPR}_{\text{GMB}} + \underbrace{Q_w(\mathbf{W}_{\text{res}})}_{\text{Quantized Residual}}. \quad (16)$$

The final reconstructed weight is obtained via the inverse transform:

$$\hat{\mathbf{W}} = \hat{\mathbf{W}}_H \mathbf{H}_n^\top. \quad (17)$$

The corresponding forward computation is

$$y = Q_w(\mathbf{W}_{\text{res}}) Q_G(x) + (\mathbf{AB} + \mathbf{L}' \mathbf{R}') \mathbf{H}_n^\top x. \quad (18)$$

Table 1. Performance on ImageNet-1K 256×256 under different settings. Best results per bit-width are highlighted.

Setting	Paradigm	Method	W/A	IS↑	FID↓	sFID↓	Precision↑
ImageNet CFG = 1.5 steps = 50	PTQ	FP	32/32	241.18	6.28	20.78	0.783
		SVD-Quant [33]	4/4	2.48	269.83	146.63	0.0070
		PTQ4DiT [57]	4/4	3.05	231.80	106.42	0.1003
		Q-DiT [4]	4/4	2.01	248.11	404.44	0.0138
		Quarot [1]	4/4	53.12	53.31	56.74	0.4134
		Baseline [61]	4/4	142.14	16.64	28.54	0.6446
		<b>TreeQ-PTQ</b>	4/4	<b>219.66</b>	<b>6.92</b>	<b>20.86</b>	<b>0.7664</b>
		SVD-Quant [33]	3/3	1.25	370.14	393.81	0.0000
		Quarot [1]	3/3	3.43	306.77	228.16	0.0171
		Baseline [61]	3/3	20.59	99.99	67.54	0.2365
		<b>TreeQ-PTQ</b>	3/3	<b>85.21</b>	<b>28.08</b>	<b>28.97</b>	<b>0.5346</b>
ImageNet CFG = 4.0 steps = 50	PEFT	QueST [56]	4/4	4.87	215.06	72.15	0.0529
		MPQ-DM [17]	4/4	76.35	22.35	35.18	0.5978
		Baseline [61]	4/4	192.13	9.87	25.05	0.7322
		<b>TreeQ-PEFT</b>	4/4	<b>206.10</b>	<b>8.69</b>	<b>23.15</b>	<b>0.7449</b>
		MPQ-DM [17]	3/3	3.45	234.69	89.27	0.1137
		Baseline [61]	3/3	128.06	16.63	29.20	0.6745
		<b>TreeQ-PEFT</b>	3/3	<b>135.84</b>	<b>14.52</b>	<b>26.49</b>	<b>0.6869</b>
		FP	32/32	478.35	19.11	21.61	0.9298
		SVD-Quant [33]	4/4	6.86	164.82	68.17	0.0413
		Quarot [1]	4/4	375.95	<b>13.05</b>	24.14	0.8178
ImageNet CFG = 4.0 steps = 50	PTQ	Baseline [61]	4/4	456.58	16.13	20.34	0.9291
		<b>TreeQ-PTQ</b>	4/4	<b>460.35</b>	17.33	<b>20.13</b>	<b>0.9330</b>
		SVD-Quant [33]	3/3	1.60	300.07	215.19	0.0063
		Quarot [1]	3/3	4.51	273.61	173.75	0.0490
		Baseline [61]	3/3	254.97	14.00	30.93	0.7160
		<b>TreeQ-PTQ</b>	3/3	<b>329.62</b>	<b>9.91</b>	<b>20.84</b>	<b>0.7943</b>
		Baseline [61]	4/4	459.80	17.91	<b>19.97</b>	0.9297
		<b>TreeQ-PEFT</b>	4/4	<b>470.10</b>	<b>17.89</b>	20.08	<b>0.9303</b>
		Baseline [61]	3/3	404.12	<b>14.49</b>	19.83	0.9180
		<b>TreeQ-PEFT</b>	3/3	<b>413.45</b>	15.03	<b>19.70</b>	<b>0.9234</b>

## 4. Experiments

### 4.1. Setup

**Datasets and Evaluation.** We evaluate pre-trained class-conditional DiT-XL/2 models at 256×256 resolution on ImageNet-1K [49]. The DDPM solver [26] with 50 sampling steps is employed for generation. To comprehensively assess the generated images, we use four widely adopted metrics: Fréchet Inception Distance (FID) [25], spatial FID (sFID) [44, 50], Inception Score (IS) [2, 50], and Precision, all computed with the ADM toolkit [12].

**Compared Methods.** We compare our TreeQ series with several leading state-of-the-art quantization approaches, covering both Post-Training Quantization (PTQ) and Parameter-Efficient Fine-Tuning (PEFT) paradigms. For **PTQ** comparison, we include general-purpose methods SVD-Quant [33] and Quarot [1], and DiT-specific methods Q-DiT [4] and PTQ4DiT [57]. For **PEFT** comparison, we include QueST [56] for low-bit PEFT quantization and MPQ-DM [17] for mixed-precision quantization. A strong RobuQ [61] baseline is included for reference as well.

**Training and Quantization Details.** All experiments are conducted with PyTorch [45] on a single NVIDIA RTX A6000-48GB GPU. For PEFT-based (QAT) methods, we

employ the QLoRA [11] strategy with the AdamW optimizer [43] at a learning rate of  $10^{-5}$  and zero weight decay. We train for 20k steps with a batch size of 24, setting QLoRA rank to 16. For methods with parallel branches (i.e., baseline RobuQ and our TreeQ), the full-precision branch is trained concurrently, as added VRAM cost and training latency are negligible. **For fair comparison, we employ per-channel weight/activation quantizers for all methods.** We keep embedding and final layers in full precision across all methods and maintain 8-bit precision for activation-activation matrix multiplication operations, which constitute minimal computation but exhibit high quantization sensitivity and instability.

**Mixed-Precision Search Configuration.** Our search space targets the 28 blocks within DiT-XL/2. We focus on layers accounting for most FLOPs: `qkv`, `proj`, `fc1`, and `fc2`. The TSS merge queue initializes following this order. We exclude `adain` layers from search due to negligible computational cost, assigning them uniform bit-width matching the target average. Candidate bit-widths are {2, 3, 4, 5}. For performance indication, we sample 64 training examples at random timesteps, perform forward passes with quantized models, and compute the MSE between their outputs and the corresponding full-precision outputs.

Table 2. Ablation Study on the maximum length of Pareto queue.

Setting	L	IS↑	FID↓	sFID↓	P↑	Time↓
CFG = 1.5 W4A4 10K Samples	4	192.35	8.31	22.26	0.7457	0.65h
	8	200.28	7.74	21.91	0.7476	2.58h
	12	198.34	8.16	22.11	0.7460	5.81h
	16	198.73	7.99	21.62	0.7517	5.16h
CFG = 1.5 W3A3 10K Samples	32	199.24	7.99	21.98	0.7497	20.64h
	4	78.43	32.85	35.99	0.5086	0.65h
	8	80.28	29.27	30.37	0.5365	2.58h
	12	87.55	26.64	29.84	0.5466	5.81h
16	94.55	23.21	27.79	0.5670	5.16h	
	32	93.93	23.82	27.92	0.5720	20.64h

## 4.2. Main Results

**Quantitative Results.** We present class-conditional generation results on ImageNet 256x256 in Tab. 1, comparing TreeQ with its baseline under PTQ and PEFT.

**Post-Training Quantization.** TreeQ establishes new state-of-the-art PTQ results across bit-widths and guidance scales. At CFG = 1.5, TreeQ achieves an FID of **6.91** in W4A4 configuration, approaching the full-precision baseline (6.28) while **surpassing all existing 4-bit PEFT methods** (9.87). Its robustness is particularly evident in extreme W3A3 quantization, maintaining 23.21 FID where conventional PTQ fails catastrophically (99.99). Under CFG = 4.0, TreeQ demonstrates superior and consistent stability, attaining **9.90 FID** at W3A3 with markedly better spatial consistency (sFID 20.83 versus 30.93).

**Parameter-Efficient Fine-Tuning.** When integrated with QLoRA, TreeQ delivers consistent improvements across all settings. At CFG = 1.5, it reduces W4A4 FID from 9.87 to **8.68** and W3A3 FID from 17.08 to **16.63**. Under CFG = 4.0, TreeQ maintains strong competitiveness with W4A4 FID of 17.32 (versus 17.91 baseline) while preserving excellent stability. These results validate that TreeQ, as a versatile and highly effective quantization framework, enhances performance across both PTQ and PEFT scenarios.

## 4.3. Ablation Study

This section presents ablation studies on TSS and GMB to evaluate key design components. Experiments were performed on ImageNet-256 to test PTQ performance. We additionally designed text-to-image (T2I) and super-resolution (SR) tasks for GMB, successfully validating its effectiveness in preserving high-frequency information.

### 4.3.1. Ablation on TSS

**Max Length.** We conducted an ablation study on the maximum length  $k$  of TSS’s Pareto queue to evaluate its PTQ performance impact. As shown in Tab. 2, we tested  $L$  values of  $\{4, 8, 12, 16, 32\}$ . Given quadratic time complexity relative to  $L$ ,  $L = 16$  provides an optimal trade-off, achieving performance comparable to  $L = 32$  with only a quarter of the computational cost. Notably, since the candidate bit-width set size is 4, whose square equals  $L$ , first-round Pareto merging requires no computation, thereby yielding additional and noticeable efficiency gains.

Table 3. Ablation on Mixed-Precision Search Algorithms. We use calibration set size  $S=64$  for TreeQ and 256 for others.

Setting	Method	IS↑	FID↓	sFID↓	P↑
CFG = 1.5 W3A3 5K Samples	baseline	20.59	103.67	83.15	0.2328
	IP+L2	60.17	49.47	61.53	0.4466
	IP+Hessian	59.27	50.28	62.34	0.4396
	IP+L1	55.42	53.15	63.94	0.4380
TreeQ	85.21	28.08	28.97	0.5346	
	FP	241.17	6.28	20.78	0.7830

Table 4. Ablation study on calibration set size.

Setting	S	IS↑	FID↓	sFID↓	P↑	iter/s↑
CFG = 1.5 W4A4 5K Samples	4	168.35	15.26	42.12	0.7004	5.96
	8	178.95	14.38	40.98	0.7280	5.89
	16	180.87	13.11	40.26	0.7372	3.04
	32	184.24	12.94	39.84	0.7423	1.52
64	194.96	12.10	39.23	0.7494	0.76	
	256	192.24	12.99	40.13	0.7374	0.19

### Comparison with Other Bit-width Allocation Schemes.

We compared different bit-width allocation schemes, testing uniform PTQ quantization and integer programming on calibration sets using L1, L2, and Hessian metrics alongside our TSS algorithm. Results in Tab. 3 demonstrate that TSS significantly outperforms other integer programming methods based on local metrics. This highlights that fully considering inter-layer interactions helps avoid optimization bias and achieve substantial improvement.

**Calibration Set Size.** We further conducted an ablation study on calibration set size to evaluate quantization performance impact. As shown in Tab. 4, progressively increasing calibration set size yields significant performance gains. We adopt a **calibration set size of 64** for optimal performance while maintaining computational efficiency.

**Analysis of Saturation.** We observed that performance does not consistently improve with larger candidate sets or queue lengths, primarily because the MSE optimization objective is not perfectly order-preserving with final metrics. However, balancing search speed and performance, we find MSE a strongly order-preserving proxy sufficiently effective. Our method can be enhanced by employing metrics with better order-preserving properties.

Table 5. Ablation studies on GMB design. 10K samples evaluated with CFG=4.0 at average W4A4.

Ablation	Method	IS↑	FID↓	sFID↓	P↑
Init. Order	GMB-first	195.71	8.32	22.57	0.7478
	LRB-first	208.77	7.53	21.68	0.7527
GMB Pos.	Pre-Hadamard	208.77	7.53	21.68	0.7527
	Post-Hadamard	219.66	6.92	20.86	0.7664
Part Num.	$r = 0$	208.36	7.46	21.54	0.7553
	$r = 4$	219.66	6.92	20.86	0.7664
	$r = 8$	214.29	6.90	20.47	0.7643
	$r = 16$	212.35	7.13	20.76	0.7735

### 4.3.2. Ablation on GMB

**Initialization Order.** We ablate two initialization strategies: (i) initializing GMB before the low-rank branch (LRB), and (ii) initializing LRB first from the Hadamard-transformed weight  $\mathbf{W}_H$ , then deriving GMB from the

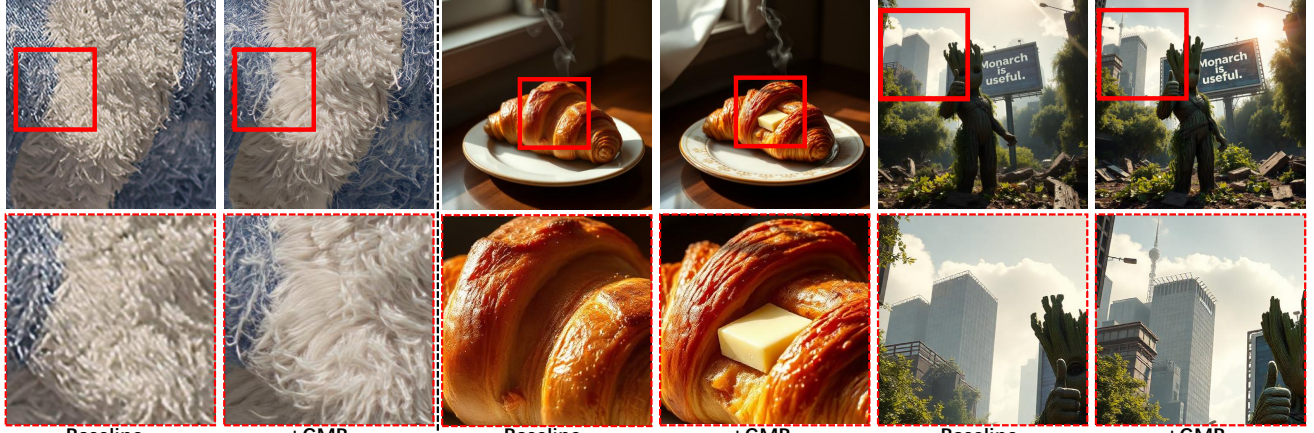


Figure 6. GMB provides more details for low-bit quantized DiT4SR (left) and FLUX-Schnell (right), advancing practical applications.

Table 6. Results on RealSR under W4A6 setting.

Method	LPIPS $\downarrow$	MUSIQ $\uparrow$	MANIQA $\uparrow$	ClipIQQA $\uparrow$	NIQE $\uparrow$
FP	0.3190	68.07	0.6610	0.5503	3.977
Baseline	<b>0.3248</b>	65.29	0.4249	0.6212	3.516
Baseline+GMB	0.3364	<b>67.10</b>	<b>0.4339</b>	<b>0.6439</b>	<b>3.788</b>

residual. Results in Tab. 5 show that (ii) yields superior performance, indicating LRB more effectively absorbs the dominant low-rank principal components, allowing GMB to better model the remaining high-rank residuals.

**Placement w.r.t. Hadamard.** We study whether GMB should be placed before or after the Hadamard transform. Experimental results favor post-transform placement. We attribute this to the Hadamard transform’s whitening effect, which promotes a more uniform weight distribution and further enables subsequent GMB to effectively retain more informative components during quantization.

**Partition Number.** We experiment with GMB’s partition number  $r$ . Using LRB with rank 16, we observe that setting **partition number**  $r = 4$  yields significant performance improvements and enhanced visual details while introducing minimal additional parameters or computational overhead.

**Ablation on High-Detail Tasks.** To further validate GMB’s generalizability and model-agnostic capabilities, we conducted supplementary experiments on high-detail tasks. For SR task, we tested on the DiT4SR [13] framework using the RealSR [3] dataset. As shown in Tab. 6, our GMB inclusion consistently improves a suite of key perceptual metrics, including MUSIQ [29], MANIQA [63], and LPIPS [65]. For T2I task, we evaluated on the FLUX-Schnell [31] model using the MJHQ-5k [66] dataset. Tab. 7 shows a similar trend, where GMB improves the FID [25] and significantly boosts perceptual scores like ImageReward [60]. The qualitative results in Fig. 6 also corroborate that GMB restores finer details. This confirms GMB’s effectiveness in preserving high-frequency fidelity across different tasks. More detailed experiment settings are given in Supplementary Material.

## 5. Limitations and Future Work

**Lack of Joint Optimization.** A limitation of our current work is the absence of a unified framework for jointly op-

Table 7. Results on MJHQ-5k under W4A4 setting.

Method	FID $\downarrow$	Image Reward $\uparrow$	CLIPQQA $\uparrow$	CLIPScore $\uparrow$	PSNR $\uparrow$
FP	18.40	0.9323	0.9399	26.54	-
Baseline	18.57	0.8617	0.9266	<b>26.34</b>	17.21
Baseline+GMB	<b>18.37</b>	<b>0.9035</b>	<b>0.9402</b>	26.29	<b>17.27</b>

timizing quantization, low-rank decomposition, and structured sparsity. Our proposed GMB branch (Sec. 3.3) serves as an effective method for introducing sparsity. However, while it has demonstrated considerable potential in its current application, we have not yet fully explored the theoretical aspects of optimizing all three components simultaneously. This remains a key direction for future research.

**Support for Diverse Quantization Kernels.** We have successfully implemented a dedicated kernel for our method in the W4A4 configuration, achieving significant gains. However, similar to challenges faced by the broader research community, efficient and publicly available implementations for other ultra-low-bit kernels—such as W2A2 and W3A3—remain scarce. We plan to develop these additional kernels in future to achieve better acceleration and demonstrate the full hardware potential of our approach.

## 6. Conclusion

In this paper, we propose **TreeQ**, a novel and comprehensive framework addressing the challenging performance degradation in ultra-low-bit Diffusion Transformers (DiTs). Our framework introduces three critical contributions: **Tree-Structured Search (TSS)**, which leverages DiT’s local dependencies for efficient topology-aware bit configuration; **Environmental Noise Guidance (ENG)**, which unifies the distinct PTQ and QAT objectives via a simple hyperparameter; and the **General Monarch Branch (GMB)**, a parallel branch that recovers high-frequency details during quantization. Extensive experiments demonstrate new state-of-the-art performance. Notably, our 4-bit PTQ achieves an FID of 6.92, remarkably close to the full-precision model and even surpassing strong PEFT baselines. This promising advancement, achieved while preserving high-frequency detail integrity, represents a significant step toward the practical deployment of low-bit DiTs.

## References

- [1] Saleh Ashkboos, Amirkeivan Mohtashami, Maximilian L. Croci, Bo Li, Pashmina Cameron, Martin Jaggi, Dan Alistarh, Torsten Hoefer, and James Hensman. Quarot: Outlier-free 4-bit inference in rotated llms. In *NeurIPS*, 2024. [6](#)
- [2] Shane Barratt and Rishi Rharma. A note on the inception score. In *ICML Workshop*, 2018. [6](#)
- [3] Jianrui Cai, Hui Zeng, Hongwei Yong, Zisheng Cao, and Lei Zhang. Toward real-world single image super-resolution: A new benchmark and a new model. In *ICCV*, 2019. [8](#)
- [4] Lei Chen, Yuan Meng, Chen Tang, Xinzhu Ma, Jinyan Jiang, Xin Wang, Zhi Wang, and Wenwu Zhu. Q-dit: Accurate post-training quantization for diffusion transformers. In *CVPR*, 2025. [6](#)
- [5] Nanxin Chen, Yu Zhang, Heiga Zen, Ron J Weiss, Mohammad Norouzi, and William Chan. Wavegrad: Estimating gradients for waveform generation. In *ICLR*, 2020. [2](#)
- [6] Zheng Chen, Yulun Zhang, Ding Liu, Bin Xia, Jinjin Gu, Linghe Kong, and Xin Yuan. Hierarchical integration diffusion model for realistic image deblurring. In *NeurIPS*, 2023. [2](#)
- [7] Florinel-Alin Croitoru, Vlad Hondu, Radu Tudor Ionescu, and Mubarak Shah. Diffusion models in vision: A survey. *TPAMI*, 2023. [2](#)
- [8] Tri Dao, Albert Gu, Matthew Eichhorn, Atri Rudra, and Christopher Ré. Learning fast algorithms for linear transforms using butterfly factorizations. In *ICML*, 2019. [2](#)
- [9] Tri Dao, Beidi Chen, Kaizhao Liang, Jiaming Yang, Zhao Song, Atri Rudra, and Christopher Ré. Pixelated butterfly: Simple and efficient sparse training for neural network models. *arXiv preprint arXiv:2112.00029*, 2021. [2](#)
- [10] Tri Dao, Beidi Chen, Nimit S Sohoni, Arjun Desai, Michael Poli, Jessica Grogan, Alexander Liu, Aniruddh Rao, Atri Rudra, and Christopher Ré. Monarch: Expressive structured matrices for efficient and accurate training. In *ICML*, 2022. [2, 5](#)
- [11] Tim Dettmers, Artidoro Pagnoni, Ari Holtzman, and Luke Zettlemoyer. Qlora: Efficient finetuning of quantized llms. In *NeurIPS*, 2023. [6](#)
- [12] Prafulla Dhariwal and Alexander Nichol. Diffusion models beat gans on image synthesis. In *NeurIPS*, 2021. [6](#)
- [13] Zheng-Peng Duan, Jiawei Zhang, Xin Jin, Ziheng Zhang, Zheng Xiong, Dongqing Zou, Jimmy Ren, Chun-Le Guo, and Chongyi Li. Dit4sr: Taming diffusion transformer for real-world image super-resolution. In *ICCV*, 2025. [8](#)
- [14] Hongxiang Fan, Thomas Chau, Stylianos I Venieris, Royson Lee, Alexandros Kouris, Wayne Luk, Nicholas D Lane, and Mohamed S Abdelfattah. Adaptable butterfly accelerator for attention-based nns via hardware and algorithm co-design. In *MICRO*, 2022. [3](#)
- [15] Marco Federici, Riccardo Del Chiaro, Boris van Breugel, Paul Whatmough, and Markus Nagel. Hadanorm: Diffusion transformer quantization through mean-centered transformations. *arXiv preprint arXiv:2506.09932*, 2025. [2](#)
- [16] Axel Feldmann and Daniel Sanchez. Spatula: A hardware accelerator for sparse matrix factorization. In *MICRO*, 2023. [2](#)
- [17] Weilun Feng, Haotong Qin, Chuanguang Yang, Zhulin An, Libo Huang, Boyu Diao, Fei Wang, Renshuai Tao, Yongjun Xu, and Michele Magno. Mpq-dm: Mixed precision quantization for extremely low bit diffusion models. In *AAAI*, 2025. [1, 2, 6](#)
- [18] Weilun Feng, Chuanguang Yang, Haotong Qin, Yuqi Li, Xiangqi Li, Zhulin An, Libo Huang, Boyu Diao, Fuzhen Zhuang, Michele Magno, Yongjun Xu, Yingli Tian, and Tingwen Huang. Mpq-dmv2: Flexible residual mixed precision quantization for low-bit diffusion models with temporal distillation. In *arXiv preprint arXiv:2507.04290*, 2025. [1, 2](#)
- [19] Daniel Y Fu, Elliot L Epstein, Eric Nguyen, Armin W Thomas, Michael Zhang, Tri Dao, Atri Rudra, and Christopher Ré. Simple hardware-efficient long convolutions for sequence modeling. In *ICML*, 2023. [3](#)
- [20] Keith G.Mills, Mohammad Salameh, Ruichen Chen, Negar Hassanpour, Wei Lu, and Di Niu. Qua<sup>2</sup>sedimo: Quantifiable quantization sensitivity of diffusion models. In *AAAI*, 2025. [1, 2](#)
- [21] Chunming He, Chengyu Fang, Yulun Zhang, Kai Li, Longxiang Tang, Chenyu You, Fengyang Xiao, Zhenhua Guo, and Xiu Li. Reti-diff: Illumination degradation image restoration with retinex-based latent diffusion model. *arXiv preprint arXiv:2311.11638*, 2023. [2](#)
- [22] Chunming He, Yuqi Shen, Chengyu Fang, Fengyang Xiao, Longxiang Tang, Yulun Zhang, Wangmeng Zuo, Zhenhua Guo, and Xiu Li. Diffusion models in low-level vision: A survey. *arXiv preprint arXiv:2406.11138*, 2024. [2](#)
- [23] Yefei He, Jing Liu, Weijia Wu, Hong Zhou, and Bohan Zhuang. Efficientdm: Efficient quantization-aware fine-tuning of low-bit diffusion models. *arXiv preprint arXiv:2310.03270*, 2023. [1, 2](#)
- [24] Yefei He, Luping Liu, Jing Liu, Weijia Wu, Hong Zhou, and Bohan Zhuang. Ptqd: Accurate post-training quantization for diffusion models. *arXiv preprint arXiv:2305.10657*, 2023. [1, 2](#)
- [25] Martin Heusel, Hubert Ransauer, Thomas Unterhiner, Bernhard Nessler, and Sepp Hochreiter. Gans trained by a two time-scale update rule converge to a local nash equilibrium. In *NeurIPS*, 2017. [5, 6, 8](#)
- [26] Jonathan Ho, Ajay Jain, and Pieter Abbeel. Denoising diffusion probabilistic models. In *NeurIPS*, 2020. [2, 6](#)
- [27] Shengchao Hu, Li Chen, Penghao Wu, Hongyang Li, Junchi Yan, and Dacheng Tao. St-p3: End-to-end vision-based autonomous driving via spatial-temporal feature learning. In *ECCV*, 2022. [2](#)
- [28] Yushi Huang, Ruihao Gong, Jing Liu, Tianlong Chen, and Xianglong Liu. Tfmq-dm: Temporal feature maintenance quantization for diffusion models. In *CVPR*, 2024. [1, 2](#)
- [29] Junjie Ke, Qifei Wang, Yilin Wang, Peyman Milanfar, and Feng Yang. Musiq: Multi-scale image quality transformer. In *ICCV*, 2021. [8](#)
- [30] Daeun Kim, Jinwoo Hwang, Changhun Oh, and Jongse Park. Mixdit: Accelerating image diffusion transformer inference with mixed-precision mx quantization. In *arXiv preprint arXiv:2504.08398*, 2025. [2](#)
- [31] Black Forest Labs. Flux.1. 2024. [8](#)

[32] Sangjun Lee, Seung-taek Woo, Jungyu Jin, Changhun Lee, and Eunhyeok Park. Amq: Enabling automl for mixed-precision weight-only quantization of large language models. *arXiv preprint arXiv:2509.12019*, 2025. 1, 2

[33] Muyang Li, Yujun Lin, Zhekai Zhang, Tianle Cai, Xiuyu Li, Junxian Guo, Enze Xie, Chenlin Meng, Jun-Yan Zhu, and Song Han. Svdquant: Absorbing outliers by low-rank components for 4-bit diffusion models. *arXiv preprint arXiv:2411.05007*, 2024. 1, 2, 6

[34] Xiuyu Li, Yijiang Liu, Long Lian, Huanrui Yang, Zhen Dong, Daniel Kang, Shanghang Zhang, and Kurt Keutzer. Q-diffusion: Quantizing diffusion models. In *ICCV*, 2023. 1, 2

[35] Yingzhou Li, Haizhao Yang, Eileen R Martin, Kenneth L Ho, and Lexing Ying. Butterfly factorization. *Multiscale Modeling & Simulation*, 13(2):714–732, 2015. 2

[36] Yuchen Li, Haoyi Xiong, Linghe Kong, Zeyi Sun, Hongyang Chen, Shuaiqiang Wang, and Dawei Yin. Mpgraf: a modular and pre-trained graphomer for learning to rank at web-scale. In *ICDM*, 2023. 2

[37] Yuchen Li, Haoyi Xiong, Linghe Kong, Rui Zhang, Fanqin Xu, Guihai Chen, and Minglu Li. Mhrr: Moocs recommender service with meta hierarchical reinforced ranking. *TSC*, 2023. 2

[38] Yangjing Li, Sheng Xu, Xianbin Cao, Xiao Sun, and Baochang Zhang. Q-dm: An efficient low-bit quantized diffusion model. In *NeurIPS*, 2023. 1, 2

[39] Yanyu Li, Huan Wang, Qing Jin, Ju Hu, Pavlo Chemerys, Yun Fu, Yanzhi Wang, Sergey Tulyakov, and Jian Ren. Snap-fusion: Text-to-image diffusion model on mobile devices within two seconds. In *NeurIPS*, 2024. 2

[40] Chang Liu, Haoning Wu, Yujie Zhong, Xiaoyun Zhang, Yanfeng Wang, and Weidi Xie. Intelligent grimm-open-ended visual storytelling via latent diffusion models. In *CVPR*, 2024. 2

[41] Kai Liu, Kaicheng Yang, Zheng Chen, Zhiteng Li, Yong Guo, Wenbo Li, Linghe Kong, and Yulun Zhang. Bimacosr: Binary one-step diffusion model leveraging flexible matrix compression for real super-resolution. In *ICML*, 2025. 5

[42] Shiwei Liu, Chen Mu, Hao Jiang, Yunzhengmao Wang, Jinshan Zhang, Feng Lin, Keji Zhou, Qi Liu, and Chixiao Chen. Hardsea: Hybrid analog-reram clustering and digital-sram in-memory computing accelerator for dynamic sparse self-attention in transformer. *IEEE Transactions on Very Large Scale Integration (VLSI) Systems*, 32(2):269–282, 2023. 3

[43] Ilya Loshchilov and Frank Hutter. Decoupled weight decay regularization. In *ICLR*, 2019. 6

[44] Charlie Nash, Jacob Menick, Sander Dieleman, and Peter W Battaglia. Generating images with sparse representations. In *arXiv preprint arXiv:2103.03841*, 2021. 5, 6

[45] Adam Paszke, Sam Gross, Francisco Massa, Adam Lerer, James Bradbury, Gregory Chanan, Trevor Killeen, Zeming Lin, Natalia Gimelshein, Luca Antiga, et al. Pytorch: An imperative style, high-performance deep learning library. In *NeurIPS*, 2019. 6

[46] William Peebles and Saining Xie. Scalable diffusion models with transformers. In *ICCV*, 2023. 2

[47] Robin Rombach, Andreas Blattmann, Dominik Lorenz, Patrick Esser, and Björn Ommer. High-resolution image synthesis with latent diffusion models. In *CVPR*, 2022. 2

[48] Olaf Ronneberger, Philipp Fischer, and Thomas Brox. U-net: Convolutional networks for biomedical image segmentation. In *MICCAI*, 2015. 2

[49] Olga Russakovsky, Jia Deng, Hao Su, Jonathan Krause, Sanjeev Satheesh, Sean Ma, Zhiheng Huang, Andrej Karpathy, Aditya Khosla, Michael Bernstein, et al. Imagenet large scale visual recognition challenge. *IJCV*, 2015. 6

[50] Tim Salimans, Ian Goodfellow, Wojciech Zaremba, Vicki Cheung, Alec Radford, and Xi Chen. Improved techniques for training gans. In *NeurIPS*, 2016. 6

[51] Yuzhang Shang, Zhihang Yuan, Bin Xie, Bingzhe Wu, and Yan Yan. Post-training quantization on diffusion models. In *CVPR*, 2023. 1, 2

[52] Yihua Shao, Deyang Lin, Fanhu Zeng, Minxi Yan, Muyang Zhang, Siyu Chen, Yuxuan Fan, Ziyang Yan, Haozhe Wang, Jingcai Guo, et al. Tr-dq: Time-rotation diffusion quantization. *arXiv preprint arXiv:2503.06564*, 2025. 1, 2

[53] Junhyuk So, Jungwon Lee, Daehyun Ahn, Hyungjun Kim, and Eunhyeok Park. Temporal dynamic quantization for diffusion models, 2023. 1, 2

[54] Siao Tang, Xin Wang, Hong Chen, Chaoyu Guan, Zewen Wu, Yansong Tang, and Wenwu Zhu. Post-training quantization with progressive calibration and activation relaxing for text-to-image diffusion models. In *ECCV*, 2024. 1, 2

[55] Ashish Vaswani, Noam Shazeer, Niki Parmar, Jakob Uszkoreit, Llion Jones, Aidan N Gomez, Łukasz Kaiser, and Illia Polosukhin. Attention is all you need. In *NeurIPS*, 2017. 2

[56] Haoxuan Wang, Yuzhang Shang, Zhihang Yuan, Junchi Wu, and Yan Yan. Quest: Low-bit diffusion model quantization via efficient selective finetuning. In *ICCV*, 2025. 1, 2, 6

[57] Junyi Wu, Haoxuan Wang, Yuzhang Shang, Mubarak Shah, and Yan Yan. Ptq4dit: Post-training quantization for diffusion transformers. In *NeurIPS*, 2024. 1, 2, 6

[58] Zhuguanyu Wu, Shihe Wang, Jiayi Zhang, Jiaxin Chen, and Yunhong Wang. Fima-q: Post-training quantization for vision transformers by fisher information matrix approximation. In *CVPR*, 2025. 2

[59] Zhuguanyu Wu, Jiayi Zhang, Jiaxin Chen, Jinyang Guo, Di Huang, and Yunhong Wang. Aphq-vit: Post-training quantization with average perturbation hessian based reconstruction for vision transformers. In *CVPR*, 2025. 2

[60] Yichuan Xu, Yifan Zhang, and Mohamed Elhoseiny. Imagereward: Learning and evaluating human preferences for text-to-image generation. In *NeurIPS*, 2023. 8

[61] Kaicheng Yang, Xun Zhang, Haotong Qin, Yucheng Lin, Kaisen Yang, Xianglong Yan, and Yulun Zhang. Robuq: Pushing bits to w1. 58a2 via robust activation quantization. *arXiv preprint arXiv:2509.23582*, 2025. 1, 2, 3, 6

[62] Ling Yang, Zhilong Zhang, Yang Song, Shenda Hong, Runsheng Xu, Yue Zhao, Wentao Zhang, Bin Cui, and Ming-Hsuan Yang. Diffusion models: A comprehensive survey of methods and applications. In *ACM Computing Surveys*, 2023. 2

[63] Sidi Yang, Tianhe Wu, Shuwei Shi, Shanshan Lao, Yuan Gong, Mingdeng Cao, Jiahao Wang, and Yujiu Yang. Maniqa: Multi-dimension attention network for no-reference image quality assessment. In *CVPRW*, 2022. [8](#)

[64] Chen Zhang, Shijie Cao, Guohao Dai, Chenbo Geng, Zhiliang Yao, Wencong Xiao, Yunxin Liu, Ming Wu, Lintao Zhang, Guangyu Sun, et al. Fine-grained structured sparse computing for fpga-based ai inference. *IEEE Transactions on Computer-Aided Design of Integrated Circuits and Systems*, 2024. [2](#)

[65] Richard Zhang, Phillip Isola, Alexei A Efros, Eli Shechtman, and Oliver Wang. The unreasonable effectiveness of deep features as a perceptual metric. In *CVPR*, 2018. [8](#)

[66] Yufei Zhang, Ming Xu, Zhaoyang Liu, Zhendong Wang, Jinyue Li, Jinjin Gu, Yu Qiao, and Chen Change Loy. Mjhq: A benchmark for high-quality text-to-image generation. In *ICCV*, 2023. [8](#)

[67] Tianchen Zhao, Xuefei Ning, Tongcheng Fang, Enshu Liu, Guyue Huang, Zinan Lin, Yan. Shengen, Guohao Dai, and Yu Wang. Mixdq: Memory-efficient few-step text-to-image diffusion models with metric-decoupled mixed precision quantization. In *ECCV*, 2024. [1](#), [2](#)

[68] Wenliang Zhao, Haolin Wang, Jie Zhou, and Jiwen Lu. Dc-solver: Improving predictor-corrector diffusion sampler via dynamic compensation. In *arXiv preprint arXiv:2409.03755*, 2024, 2024. [2](#)

[69] Xinyu Zheng, Xianglong Liu, Yichen Bian, Xudong Ma, Yulun Zhang, Jiakai Wang, Jingyang Guo, and Haotong Qin. Bidm: Pushing the limit of quantization for diffusion models. In *NeurIPS*, 2024. [1](#), [2](#)

[70] Xinyu Zheng, Xianglong Liu, Haotong Qin, Xudong Ma, Mingyuan Zhang, Haojie Hao, Jiakai Wang, Zixiang Zhao, Jingyang Guo, and Michele Magno. Binarydm: Accurate weight binarization for efficient diffusion models. In *ICLR*, 2025. [1](#), [2](#)

[71] Qiuling Zhu, Tobias Graf, H Ekin Sumbul, Larry Pileggi, and Franz Franchetti. Accelerating sparse matrix-matrix multiplication with 3d-stacked logic-in-memory hardware. In *IEEE High Performance Extreme Computing Conference (HPEC)*, 2013. [2](#)

[72] Ling Zhuo and Viktor K Prasanna. Sparse matrix-vector multiplication on fpgas. In *Proceedings of the 2005 ACM/SIGDA 13th international symposium on Field-programmable gate arrays*, pages 63–74, 2005. [2](#)